

# Freeze, Diffuse, Decode: Geometry-Aware Adaptation of Pretrained Transformer Embeddings for Antimicrobial Peptide Design

Pankhil Gawade<sup>\*1,2</sup>, Adam Izdebski<sup>\*1,2</sup>, Myriam Lizotte<sup>3</sup>, Kevin R. Moon<sup>4</sup>, Jake S. Rhodes<sup>5</sup>, Guy Wolf<sup>1,3</sup>, and Ewa Szczyrek<sup>1,6</sup>

<sup>1</sup> Institute of AI for Health, Helmholtz Munich

<sup>2</sup> School of Computation, Information and Technology, Technical University of Munich

<sup>3</sup> Mila - Quebec AI institute; Univ. de Montreal

<sup>4</sup> Dept. Mathematics & Statistics, Utah State University

<sup>5</sup> Department of Statistics, Brigham Young University

<sup>6</sup> Faculty of Mathematics, Informatics and Mechanics, University of Warsaw

{gawade.pankhil,adam.izdebski,ewa.szczyrek}@helmholtz-munich.de

**Abstract.** Pretrained transformers provide rich, general-purpose embeddings, which are transferred to downstream tasks. However, current transfer strategies: fine-tuning and probing, either distort the pretrained geometric structure of the embeddings or lack sufficient expressivity to capture task-relevant signals. These issues become even more pronounced when supervised data are scarce. Here, we introduce FREEZE, DIFFUSE, DECODE (FDD), a novel diffusion-based framework that adapts pretrained embeddings to downstream tasks while preserving their underlying geometric structure. FDD propagates supervised signal along the intrinsic manifold of frozen embeddings, enabling a geometry-aware adaptation of the embedding space. Applied to antimicrobial peptide design, FDD yields low-dimensional, predictive, and interpretable representations that support property prediction, retrieval, and latent-space interpolation.

**Keywords:** Representation Learning · Diffusion Maps · Antimicrobial Peptide Discovery.

## 1 Introduction

Molecular representation learning is fundamental to modern computational chemistry and drug discovery. Embedding molecular structures into high-dimensional features that capture structural and chemical properties enables downstream tasks such as molecular property prediction, molecule retrieval, and chemical space exploration. Recently, pretrained transformers have been reshaping molecular machine learning by providing transferable embeddings that are increasingly leveraged across diverse downstream tasks [7,6,36].

---

<sup>\*</sup> These authors contributed equally.

However, the two dominant paradigms for transferring pretrained embeddings to downstream tasks, fine-tuning and probing, exhibit inherent limitations. Fine-tuning offers flexibility and strong task-specific performance on in-distribution data, but often distorts the geometry of pretrained embeddings, compromising robustness under distribution shifts and leading to catastrophic forgetting [1,17]. Probing, on the other hand, preserves the pretrained feature space, but lacks the expressive power needed to capture nonlinear, task-specific structure [3,24]. These limitations become amplified with limited downstream data, since scarce supervision exacerbates overfitting and a drift from the geometry of the pretrained embeddings, while further restricting probing from capturing task-relevant structure.

To address this gap, we introduce FREEZE, DIFFUSE, DECODE (FDD), a diffusion-based framework for adapting pretrained transformer embeddings to downstream tasks *without* fine-tuning. Building on the hypothesis that pretrained embeddings encode a meaningful latent geometric structure, FDD propagates limited task-specific supervision along the intrinsic manifold of frozen transformer embeddings. This aligns the geometry of the pretrained embeddings with task-specific signal, yielding low-dimensional representations that preserve generality while enhancing downstream performance. Our contributions are:

- We propose FREEZE, DIFFUSE, DECODE (FDD), a diffusion-based framework for adapting frozen transformer embeddings to task-specific representations.
- We show that FDD yields predictive, interpretable representations for molecular property prediction and peptide retrieval.
- We demonstrate that FDD supports smooth latent-space interpolations that enable the discovery of novel antimicrobial peptides.

## 2 Related Work

### 2.1 Molecular Representation Learning

Molecular representation learning has shifted from hand-crafted descriptors to large-scale pre-trained models that learn representations directly from sequences, graphs, or 3D structures. Transformer-based molecular and protein language models, including Uni-Mol [36], Mol-Found [33], and ESM-2 [20], produce rich molecular embeddings that are transferable to a broad range of downstream tasks, from property prediction to docking and binding affinity estimation.

The utility of general-purpose pretrained embeddings ultimately depends on how effectively they can be transferred to downstream tasks. Most adaptation strategies rely on fine-tuning or probing frozen features. Although fine-tuning is expressive, growing evidence shows that it reshapes the embedding geometry, degrades robustness, and can underperform w.r.t. probing baselines, particularly when downstream data is scarce [17,1,25]. On the other hand, probing preserves the geometry of the pretrained embeddings but lacks the expressivity needed to capture complex task structure. Probing studies in NLP and vision show that linear classifiers often underestimate the information encoded in pretrained

embeddings [3,15,34]. Similar patterns appear in molecular modeling, where shallow models trained on frozen embeddings frequently underperform on property prediction benchmarks [12,10,24].

## 2.2 Geometry-Aware Representation Learning

A long line of work in manifold learning aims to construct representations that reflect the intrinsic geometry of high-dimensional data. Diffusion Maps [8] introduced a principled framework for building diffusion operators over sample affinities and extracting low-dimensional coordinates that preserve global topology while denoising local neighborhoods. Building on this idea, PHATE [23] developed a diffusion-potential representation that further stabilizes local neighborhoods and captures both global and local data structure. More recently, RF-PHATE [26] and related supervised variants incorporate task information into the diffusion kernel itself. By using random forest-based affinities or label-aware similarity measures, these methods bias the underlying manifold toward task-relevant directions while maintaining the global geometric structure inherited from the data. Finally, RFAE [28] leverages random forest-based affinities to build label-informed diffusion operators that produce embeddings well suited for complex biological datasets.

## 2.3 Geometry-Aware Adaptation of Pretrained Embeddings

To the best of our knowledge, FDD provides the first geometry-aware downstream adaptation framework for pretrained molecular embeddings. It closes the gap between the expressivity of fine-tuning and the geometry preservation of probing by treating frozen transformer embeddings as a manifold and adapting them directly in feature space through a supervised diffusion process, yielding low-dimensional representations that remain close to the pretrained space while selectively amplifying task-relevant directions.

# 3 Freeze, Diffuse, Decode

## 3.1 Overview

Pretrained embeddings encode meaningful latent geometric structure that reflects regularities of the chemical space. At its core, FDD constructs a diffusion process that propagates task-specific signal across the pretrained manifold, producing representations that remain faithful to the original geometric structure while emphasizing task-relevant directions, even when task-specific data is scarce. These adapted representations can then be decoded for prediction, retrieval, or generation, enabling task alignment without modifying the pretrained weights. FDD operates in three steps (Fig. 1). The *Freeze* step extracts high-dimensional embeddings from a pretrained transformer model without updating its parameters. By fixing the model weights, this step preserves the general structural knowledge encoded during large-scale pretraining.

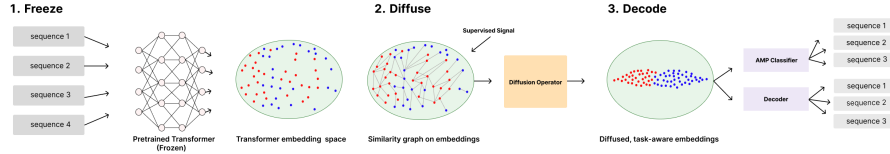


Fig. 1: Overview of the FDD framework.

The *Diffuse* step propagates task-specific information across the pretrained embedding manifold by spreading supervision through the local similarity structure of the frozen embeddings. Following the intuition of diffusion maps [8], this process aggregates local geometric relationships into a smooth global representation that remains faithful to the pretrained embedding space. Through this supervised diffusion, the adapted representations become selectively oriented along task-relevant directions while preserving the underlying geometric structure of the pretrained embeddings.

The *Decode* step maps the learned geometry-aware representations into downstream task-specific output. Once low-dimensional, geometry-aware coordinates are obtained, lightweight decoders are trained to map these latent embeddings to downstream targets, such as molecular properties, retrieval scores, or reconstructed transformer embeddings. In predictive settings, this decoder can take the form of a regression or classification head, while in generative contexts, it translates latent vectors into molecular or peptide sequences via the pretrained transformer’s decoder.

### 3.2 Methodology

Let  $\mathcal{X}$  denote the *input space* of all sequences, e.g., all chains of amino acids. Let a *sequence*  $\mathbf{x}_n = (x_{n,1}, \dots, x_{n,T}) \in \mathcal{X}$  be defined as a sequence of *tokens*  $x_t$ . The input set  $\mathcal{X}$  provides the foundation for constructing sequence embeddings that can be compared and manipulated geometrically.

**Freeze** The first step in our framework, the *Freeze* step, begins with a pretrained transformer *encoder*  $f_\theta : \mathcal{X} \rightarrow \mathbb{R}^D$  that maps sequences  $\mathbf{x} \in \mathcal{X}$  into high-dimensional *embeddings*  $\mathbf{e} := f_\theta(\mathbf{x}) \in \mathbb{R}^D$ , which captures a general task-agnostic structure learned during pretraining. For our implementation, we use Hyformer [16], a joint transformer model that integrates a bidirectional encoder and an autoregressive decoder within a shared architecture through an alternating attention mechanism. By alternating between causal and bidirectional masks during pretraining, Hyformer learns molecular representations that capture both generative structure and predictive semantics. This design makes it suitable for the *Freeze* step, as it produces rich embeddings that preserve chemical regularities useful for downstream diffusion-based adaptation.

**Diffuse** For the *Diffuse* step, we introduce a *projection*  $g : \mathbb{R}^D \mapsto \mathbb{R}^d$  that maps high-dimensional frozen embeddings extracted during the *Freeze* step into geometry-aware *latent representations*  $\mathbf{z} := (g \circ f_\theta)(\mathbf{x}) \in \mathbb{R}^d$ . The projection  $g$  reduces the embedding dimensionality while preserving the manifold structure of the pretrained embedding space. We implement  $g$  using an autoencoder regularized by geometry-aware diffusion maps [8,23] and random forest-based affinity supervision [26], following the design principles of geometry-regularized autoencoders [11,2]. In consequence,  $g$  produces low-dimensional representations that align with both the latent geometry of the transformer embeddings and the task-specific signal. Specifically, the *Diffuse* step propagates task-specific information across the manifold embedding via a random walk governed by a supervised similarity kernel  $\mathbf{K}$ . This kernel encodes pairwise affinities between samples, capturing the local geometric structure while aligning it with the supervised objective. A Markov chain, or diffusion operator, is then constructed by row-wise normalization of  $\mathbf{K}$ , defining transition probabilities that reflect these local relationships. Iterative application of the diffusion operator integrates local interactions over multiple steps, producing a global representation of the data manifold oriented along task-relevant directions. Conceptually, this process resembles integrating local dynamics in a differential system, yielding a smooth, multiscale description of the embedding space that preserves both geometric and supervised structure.

**Decode** Finally, the *Decode* step maps the geometry-aware latent representation space of FDD to a downstream specific output, which is either prediction or generation. For prediction (and retrieval), a predictive model  $Pred_\phi : \mathbb{R}^d \mapsto \mathcal{Y}$  is fitted on latent representations  $\mathbf{z} \in \mathbb{R}^d$ , allowing the model to map geometry-aware representations directly to task-specific labels  $\hat{y} = Pred_\phi(\mathbf{z})$ . Analogously, for sequence generation (and reconstruction), a decoder  $Dec_\phi : \mathbb{R}^d \mapsto \mathbb{R}^D$  is fitted on the latent representations  $\mathbf{z} \in \mathbb{R}^d$ , decoding latent representations back to the transformer’s embedding space  $\mathbf{e} = Dec_\phi(\mathbf{z}) \in \mathbb{R}^D$ , which are then subsequently passed through the frozen transformer decoder to map the embeddings back to the input space  $\mathcal{X}$ . In our implementation, to further align the *Decode* step with the geometry-aware representations, we use the decoder of the diffusion regularized AE learned during the *Diffuse* step as the decoder  $Dec_\phi$ .

### 3.3 Latent Space Interpolation via Neural ODEs

To explore continuous interpolation in the latent space, we define an ordinary differential equation (ODE) over the diffusion coordinates  $\mathbf{z}(t) \in \mathbb{R}^d$

$$\frac{d\mathbf{z}(t)}{dt} = h(\mathbf{z}(t), t; \psi),$$

where  $h : \mathbb{R}^d \times [0, 1] \rightarrow \mathbb{R}^d$  is a learnable vector field parameterized by a neural network with weights  $\psi$ , trained with Sinkhorn loss [9,13]. Solving the above ODE produces smooth interpolation paths  $\{\mathbf{z}(t) \mid t \in [0, 1]\}$  in the latent space, enabling

transformation of latent representations from one region to the other. Specifically, at each training iteration, we sample a mini-batch  $\{\mathbf{z}_m(0)\}_{m=1}^M$  from one region in the latent and a target mini-batch  $\{\mathbf{z}_m(1)\}_{m=1}^M$  from the other. Next, we compute trajectory points  $\mathbf{z}_m(t)$  via the ODE solver and evaluate the accelerated Sinkhorn Loss  $\mathcal{L}_{\text{Sinkhorn}}$ , with  $\varepsilon = 0.1$  regularization for stable gradients, given by

$$\mathcal{L}_{\text{Sinkhorn}} = \text{OT}_\varepsilon(\mu, \nu) - \frac{1}{2} \left[ \text{OT}_\varepsilon(\mu, \mu) + \text{OT}_\varepsilon(\nu, \nu) \right], \quad (1)$$

where  $\text{OT}_\varepsilon$  is the entropy-regularized optimal transport term

$$\text{OT}_\varepsilon(\mu, \nu) = \min_{P \in \Pi(\mu, \nu)} \left[ \sum_{i,j} P_{ij} \|\mathbf{z}_i - \mathbf{z}_j\|^2 + \varepsilon \text{KL}(P \|\mu \otimes \nu) \right], \quad (2)$$

where  $\mu, \nu$  are respectively the source and target marginal probability distributions (in our case, uniform distributions over the sample trajectory points  $\{\mathbf{z}_m(0)\}$  or the targets  $\{\mathbf{z}_m(1)\}$  respectively),  $\{\mathbf{z}_i\} \sim \mu$  and  $\{\mathbf{z}_j\} \sim \nu$  are samples from the two probability distributions,  $P$  is a matrix representing a transport plan subject to marginal constraints defined by  $\Pi$ , and  $\text{KL}(P \|\mu \otimes \nu)$  denotes the KL-divergence of  $P$  with respect to the product measure  $\mu \otimes \nu$ . Finally, we jointly optimize the neural network parameters by backpropagating through both the ODE integration (adjoint sensitivity) and the Sinkhorn computation. Once trained, latent codes  $\mathbf{z}_m(t)$  are passed through our decoding pipeline, yielding novel peptide sequences.

## 4 Experiments

We demonstrate the utility of the proposed FDD framework by showing that the embeddings derived from pretrained transformers can be adapted to various downstream tasks in antimicrobial peptide (AMP) discovery, including predictive modeling (Section 4.1), peptide retrieval (Section 4.2), and latent-space interpolation (Section 4.3). Our results indicate that FDD yields unified representations of the pretrained embeddings with task-specific supervision, enabling robust and interpretable adaptation of pretrained transformer embeddings.

*Setup.* We evaluate the performance of FDD across a variety of datasets, including: antimicrobial activity against *E. coli* bacteria strain [30] and a classification dataset of AMPs [32]. To obtain pretrained embeddings, we use HYFORMER [16], a joint transformer model scaled to 8M parameters and pretrained on 1.4M peptide sequences, which are short chains of amino acids, from combined Peptipedia [4], AMPSphere [29], and UniProt [31] datasets. For consistency, frozen embeddings from HYFORMER serve as inputs to all embedding adaptation methods.

### 4.1 FDD improves upon the predictive performance of pretrained transformer embeddings

To evaluate the predictive performance of geometry-aware representations produced by FDD, we perform a binary classification task of antimicrobial peptides

Table 1: Predictive performance of pretrained transformer embeddings adapted using different methods, as measured by AUC ( $\uparrow$ ) across all transformer layers (L0-L8). Best results are marked **bold**, best result across each of the methods is underlined.

Method	L0	L1	L2	L3	L4	L5	L6	L7	L8
None	0.546	0.822	0.827	0.818	0.825	0.835	<u>0.844</u>	0.842	0.835
AE	0.496	0.518	0.450	<u>0.578</u>	0.486	0.485	0.482	0.483	0.453
T-SNE	0.550	<u>0.704</u>	0.661	0.681	0.651	0.683	0.672	0.674	0.651
FDD (ours)	0.696	0.957	0.962	0.960	0.961	<b>0.965</b>	<b>0.965</b>	0.962	0.961

against the *E. coli* strain using the dataset of [30]. Specifically, we extract layer-wise transformer embeddings of the training dataset and adapt them using one of the four methods: None, which uses raw frozen embeddings without adaptation; AE [14], an autoencoder trained to reconstruct transformer embeddings; T-SNE [21], an unsupervised dimensionality reduction method; and FDD (ours), which incorporates classification labels to learn geometry-aware representations. Finally, using an MLP classifier, we probe each layer’s adapted representations.

Geometry-aware adaptation using FDD (ours) outperforms all other adaptation methods in terms of predictive performance, as measured by AUC in Table 1. In particular, FDD increases the predictive accuracy obtained from transformer embeddings across all layers, with the highest AUC (0.965) at intermediate layers (L5–L6). To further investigate this phenomenon, Table 2 shows the AE’s reconstruction loss across the transformer layers. Here, we see that the baseline AE reconstruction loss (MSE) increases with layer depth, reflecting greater feature complexity in deeper transformer layers. Geometry-aware adaptation in FDD effectively leverages this complexity, yielding improved predictive performance for higher complexity layers, with Pearson correlation coefficient between the AUC for FDD and the reconstruction error equal to 0.51.

Table 2: Reconstruction loss (MSE) of an autoencoder (AE) trained on pretrained transformer embeddings across successive transformer layers (L0-L8).

	L0	L1	L2	L3	L4	L5	L6	L7	L8
Reconstruction Loss	0.0003	0.0291	0.0935	0.1553	0.2107	0.2699	0.3254	0.3901	0.1030

#### 4.2 FDD allows for a successful retrieval of novel active peptides

To evaluate the ability of FDD to retrieve novel antimicrobial peptides, we train a predictor on the FDD embeddings of the dataset from [32] and use it to retrieve antimicrobial peptides from the held-out classification dataset of [30], used in Section 4.1. In particular, we encode each peptide into a latent representation produced with FDD. Retrieval is performed

Table 3: Peptide retrieval performance, as measured by  $P_{amp}$ .

Method	$P_{amp}$ ( $\uparrow$ )
RF	0.80
HydrAMP	0.83
AMPSanner	0.89
AMPLify	0.89
<b>FDD (ours)</b>	<b>0.90</b>

by ranking candidates according to their proximity to known active regions, i.e., by using  $k$ NN ( $k=5$ ) classification. This setup aims to test whether FDD yields representations that capture biological similarity and remain robust when applied to novel peptides not seen during training.

We compare the  $k$ NN-based FDD classifier against state-of-the-art AMP classifiers, including: random forest trained on physicochemical descriptors (RF), HydrAMP [30], AMPScanner [35] and AMPlify [19]. All models are evaluated on the same held-out dataset using the probability of retrieving an antimicrobial peptide  $P_{\text{amp}}$ , as the retrieval accuracy metric.

As shown in Table 3, FDD achieves the highest retrieval performance ( $P_{\text{amp}} = 0.90$ ), outperforming all other classifiers. These results are supported by the visualization of the learned embedding space in Figure 2, which clearly separates active and inactive peptides, enabling accurate identification of novel active sequences through nearest-neighborhood classification. These results indicate that FDD provides an interpretable and robust latent representation learning method.

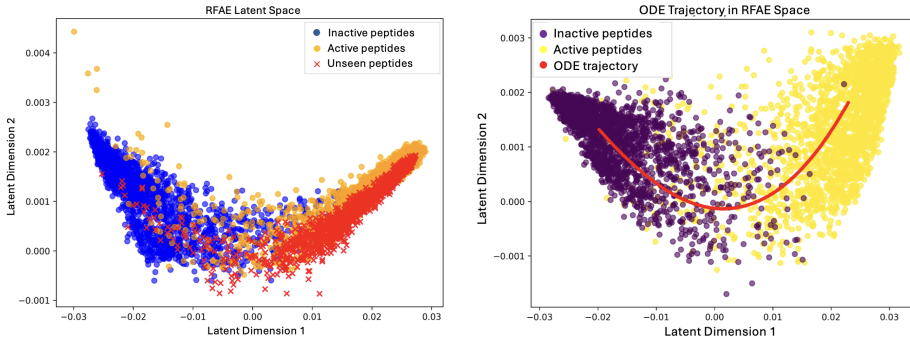


Fig. 2: Embedding space for AMP/NonAMP retrieval using FDD. Red points indicate active peptide embeddings from the held-out dataset projected into FDD latent space.

Fig. 3: Interpolated trajectory in the FDD latent space between non-AMP and AMP regions.

#### 4.3 FDD enables smooth latent-space interpolation

Finally, we investigate whether FDD enables smooth latent-space interpolation between AMP and non-AMP peptides. For this, we use the dataset from [32] and map all peptides into the FDD latent representation space. Specifically, we select a single non-AMP latent vector  $\mathbf{z}_0$  and a Neural ODE [5] that integrates a continuous trajectory from  $\mathbf{z}_0$  towards the AMP manifold, using Sinkhorn optimal transport loss [22] to align the evolving distribution with that of active peptides (Figure 3). Intermediate points along the trajectory are decoded back to peptide sequences via a learned MLP mapping, enabling an analysis of the changes in physicochemical descriptors across interpolation steps.

Peptides decoded along the learned interpolation path exhibit a smooth and monotonic transition in physicochemical descriptors that correlate with antimicrobial properties of peptides (Figure 4). As an example, net charge increases from near-neutral to cationic (Figure 4 (a)), isoelectric point rises accordingly (Figure 4 (b)), and the hydrophobic amino-acid ratio grows, reflecting stronger membrane affinity typical of decoded AMPs (Figure 4 (c)). These results indicate that geometry-aware representations extracted with FDD capture a biologically meaningful, smooth manifold structure, where latent-space interpolation corresponds to a gradual acquisition of antimicrobial characteristics.

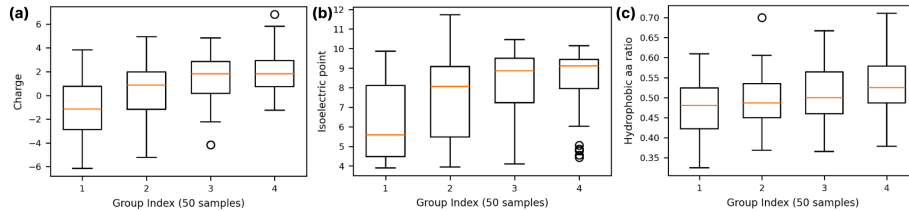


Fig. 4: Evolution of physicochemical descriptors along the latent interpolation path: (a) net charge, (b) isoelectric point, and (c) hydrophobic amino-acid ratio. All descriptors steadily increase across the interpolation path, indicating a smooth transition from non-AMP to AMP-like regions in latent space.

## 5 Conclusions and Future Work

In this work, we introduced FREEZE, DIFFUSE, DECODE (FDD), a diffusion-based framework for adapting pretrained transformer embeddings to downstream molecular tasks without fine-tuning. Latent representations extracted with FDD preserve the geometric structure of the embeddings learned during pretraining while aligning them with task-specific supervision. Across property prediction, peptide retrieval, and latent space interpolation benchmarks, our method yields smooth and predictive embeddings, demonstrating that geometry-aware adaptation can successfully serve as an alternative to parameter-based fine-tuning.

Future work will focus on extending FDD to multi-modal settings, where molecular embeddings are jointly aligned with complementary data modalities such as cellular morphology or transcriptomics [18]. In this context, geometry-aware diffusion offers a principled mechanism to integrate supervision across heterogeneous feature spaces while preserving the structural priors specific to each modality. Such an extension would enable unified modeling of molecular function and phenotype, advancing multi-domain representation learning.

**Acknowledgments.** This project has received funding from the European Research Council (ERC) under the European Funding Union’s Horizon 2020 research and innovation programme (grant agreement No 810115–DOG-AMP) [E.S.]; a FRQNT doctoral scholarship and Mitacs-Globalink travel award [M.L.]; a Canada CIFAR AI chair (via Mila) and Humboldt research fellowship [G.W.]; and an IVADO visiting scholar award [K.M.]

**Disclosure of Interests.** Projects in Szczurek lab at the University of Warsaw are co-funded by Merck KGaA.

## References

1. Andreassen, A., Bahri, Y., Neyshabur, B., Roelofs, R.: The evolution of out-of-distribution robustness throughout fine-tuning. arXiv preprint arXiv:2106.15831 (2021)
2. Aumon, A., Ni, S., Lizotte, M., Wolf, G., Moon, K.R., Rhodes, J.S.: Random forest autoencoders for guided representation learning (2025), <https://arxiv.org/abs/2502.13257>
3. Belinkov, Y.: Probing classifiers: Promises, shortcomings, and advances. Computational Linguistics **48**(1), 207–219 (Mar 2022). [https://doi.org/10.1162/coli\\_a\\_00422](https://doi.org/10.1162/coli_a_00422), <https://aclanthology.org/2022.cl-1.7/>
4. Cabas-Mora, G., Daza, A., Soto-García, N., Garrido, V., Alvarez, D., Navarrete, M., Sarmiento-Varón, L., Sepúlveda Yañez, J.H., Davari, M.D., Cadet, F., Olivera-Nappa, Á., Uribe-Paredes, R., Medina-Ortiz, D.: Peptipedia v2.0: A peptide sequence database and user-friendly web platform. a major update (Jul 2024), bioRxiv
5. Chen, R.T.Q., Rubanova, Y., Bettencourt, J., Duvenaud, D.: Neural ordinary differential equations (2019), <https://arxiv.org/abs/1806.07366>
6. Chithrananda, S., Grand, G., Ramsundar, B.: Chemberta: large-scale self-supervised pretraining for molecular property prediction. arXiv preprint arXiv:2010.09885 (2020)
7. Chuang, K.V., Gunsalus, L.M., Keiser, M.J.: Learning molecular representations for medicinal chemistry: miniperspective. Journal of Medicinal Chemistry **63**(16), 8705–8722 (2020)
8. Coifman, R.R., Lafon, S.: Diffusion maps. Applied and Computational Harmonic Analysis **21**(1), 5–30 (2006). <https://doi.org/https://doi.org/10.1016/j.acha.2006.04.006>, <https://www.sciencedirect.com/science/article/pii/S1063520306000546>, special Issue: Diffusion Maps and Wavelets
9. Cuturi, M.: Sinkhorn distances: Lightspeed computation of optimal transportation distances (2013), <https://arxiv.org/abs/1306.0895>
10. Dey, V., Ning, X.: Enhancing molecular property prediction with auxiliary learning and task-specific adaptation (2024), <https://arxiv.org/abs/2401.16299>
11. Duque, A.F., Morin, S., Wolf, G., Moon, K.R.: Geometry regularized autoencoders. IEEE Transactions on Pattern Analysis and Machine Intelligence **45**(6), 7381–7394 (2023). <https://doi.org/10.1109/TPAMI.2022.3222104>
12. Formont, P., Jeannin, H., Piantanida, P., Ayed, I.B.: A strong baseline for molecular few-shot learning (2025), <https://arxiv.org/abs/2404.02314>
13. Genevay, A., Peyre, G., Cuturi, M.: Learning generative models with sinkhorn divergences. In: Storkey, A., Perez-Cruz, F. (eds.) Proceedings of the Twenty-First International Conference on Artificial Intelligence and Statistics. Proceedings of Machine Learning Research, vol. 84, pp. 1608–1617. PMLR (09–11 Apr 2018), <https://proceedings.mlr.press/v84/genevay18a.html>
14. Goodfellow, I., Bengio, Y., Courville, A.: Autoencoders. deep learning (2016)
15. Hewitt, J., Manning, C.D.: A structural probe for finding syntax in word representations. In: Burstein, J., Doran, C., Solorio, T. (eds.) Proceedings of the 2019 Conference of the North American Chapter of the Association for Computational Linguistics: Human Language Technologies, Volume 1 (Long and

Short Papers). pp. 4129–4138. Association for Computational Linguistics, Minneapolis, Minnesota (Jun 2019). <https://doi.org/10.18653/v1/N19-1419>, <https://aclanthology.org/N19-1419/>

16. Izdebski, A., Olszewski, J., Gawade, P., Koras, K., Korkmaz, S., Rauscher, V., Tomczak, J.M., Szczerk, E.: Synergistic benefits of joint molecule generation and property prediction (2025), <https://arxiv.org/abs/2504.16559>
17. Kumar, A., Raghunathan, A., Jones, R., Ma, T., Liang, P.: Fine-tuning can distort pretrained features and underperform out-of-distribution. arXiv preprint arXiv:2202.10054 (2022)
18. Lederman, R.R., Talmon, R.: Learning the geometry of common latent variables using alternating-diffusion. *Applied and Computational Harmonic Analysis* **44**(3), 509–536 (2018). <https://doi.org/https://doi.org/10.1016/j.acha.2015.09.002>, <https://www.sciencedirect.com/science/article/pii/S1063520315001190>
19. Li, C., Sutherland, D., Hammond, S.A., Yang, C., Taho, F., Bergman, L., Houston, S., Warren, R.L., Wong, T., Hoang, L.M.N., Cameron, C.E., Helbing, C.C., Birol, I.: AMPlify: attentive deep learning model for discovery of novel antimicrobial peptides effective against WHO priority pathogens. *BMC Genomics* **23**(1), 77 (Jan 2022)
20. Lin, Z., Akin, H., Rao, R., et al.: Esm-2: Evolutionary-scale modeling for large-scale protein understanding. *bioRxiv* (2023)
21. Maaten, L.v.d., Hinton, G.: Visualizing data using t-sne. *Journal of machine learning research* **9**(Nov), 2579–2605 (2008)
22. Marino, S.D., Gerolin, A.: Optimal transport losses and sinkhorn algorithm with general convex regularization (2020), <https://arxiv.org/abs/2007.00976>
23. Moon, K.R., van Dijk, D., Wang, Z., Gigante, S., Burkhardt, D.B., Chen, W.S., Yim, K., van den Elzen, A., Hirn, M.J., Coifman, R.R., Ivanova, N.B., Wolf, G., Krishnaswamy, S.: Visualizing structure and transitions in high-dimensional biological data. *Nature Biotechnology* **37**(12), 1482–1492 (Dec 2019)
24. Praski, M., Adamczyk, J., Czech, W.: Benchmarking pretrained molecular embedding models for molecular representation learning (2025), <https://arxiv.org/abs/2508.06199>
25. Rajaei, S., Pilehvar, M.T.: How does fine-tuning affect the geometry of embedding space: A case study on isotropy. In: Conference on Empirical Methods in Natural Language Processing (2021), <https://api.semanticscholar.org/CorpusID:237485161>
26. Rhodes, J.S., Aumon, A., Morin, S., Girard, M., Larochelle, C., Lahav, B., Brunet-Ratnasingham, E., Zhang, W., Cutler, A., Zhou, A., Kaufmann, D.E., Zandee, S., Prat, A., Wolf, G., Moon, K.R.: Gaining biological insights through supervised data visualization. *bioRxiv* (2023). <https://doi.org/10.1101/2023.11.22.568384>, <https://www.biorxiv.org/content/early/2023/11/23/2023.11.22.568384>
27. Rhodes, J.S., Cutler, A., Moon, K.R.: Geometry- and accuracy-preserving random forest proximities. *IEEE Transactions on Pattern Analysis and Machine Intelligence* **45**(9), 10947–10959 (2023). <https://doi.org/10.1109/TPAMI.2023.3263774>
28. Rhodes, J.S., Rustad, A.G.: Random forest-supervised manifold alignment. In: 2024 IEEE International Conference on Big Data (BigData). pp. 3309–3312 (2024). <https://doi.org/10.1109/BigData62323.2024.10825663>
29. Santos-Júnior, C.D., Torres, M.D.T., Duan, Y., Rodríguez Del Río, Á., Schmidt, T.S.B., Chong, H., Fullam, A., Kuhn, M., Zhu, C., Houseman, A., Somborski, J., Vines, A., Zhao, X.M., Bork, P., Huerta-Cepas, J., de la Fuente-Nunez, C., Coelho,

L.P.: Discovery of antimicrobial peptides in the global microbiome with machine learning. *Cell* **187**(14), 3761–3778.e16 (Jul 2024)

- 30. Szymczak, P., Mozejko, M., Grzegorzek, T., Jurczak, R., Bauer, M., Neubauer, D., Sikora, K., Michalski, M., Sroka, J., Setny, P., Kamysz, W., Szczurek, E.: Discovering highly potent antimicrobial peptides with deep generative model HydrAMP. *Nat. Commun.* **14**(1), 1453 (Mar 2023)
- 31. UniProt Consortium: UniProt: The universal protein knowledgebase in 2025. *Nucleic Acids Res.* **53**(D1), D609–D617 (Jan 2025)
- 32. Veltri, D., Kamath, U., Shehu, A.: Deep learning improves antimicrobial peptide recognition. *Bioinformatics* **34**(16), 2740–2747 (Aug 2018)
- 33. Wang, B., Zhang, J., Zhao, L., et al.: Molfound: Self-supervised molecular representation learning for property prediction. In: *NeurIPS* (2022)
- 34. White, J.C., Pimentel, T., Saphra, N., Cotterell, R.: A non-linear structural probe. In: Toutanova, K., Rumshisky, A., Zettlemoyer, L., Hakkani-Tur, D., Beltagy, I., Bethard, S., Cotterell, R., Chakraborty, T., Zhou, Y. (eds.) *Proceedings of the 2021 Conference of the North American Chapter of the Association for Computational Linguistics: Human Language Technologies*. pp. 132–138. Association for Computational Linguistics, Online (Jun 2021). <https://doi.org/10.18653/v1/2021.naacl-main.12>, <https://aclanthology.org/2021.naacl-main.12>
- 35. Yang, C.H., Chen, Y.L., Cheung, T.H., Chuang, L.Y.: Multi-objective optimization accelerates the de novo design of antimicrobial peptide for staphylococcus aureus. *International Journal of Molecular Sciences* **25**, 13688 (12 2024). <https://doi.org/10.3390/ijms252413688>
- 36. Zhou, J., Luo, Y., Li, Y., et al.: Uni-mol: A universal 3d molecular representation learning framework. *Nature Communications* **14**, 4074 (2023)

**Supplementary Material**  
**for**  
**Freeze, Diffuse, Decode: Geometry-Aware**  
**Adaptation of**  
**Pretrained Transformer Embeddings for**  
**Antimicrobial Peptide Design**

Pankhil Gawade<sup>1,2,\*</sup>, Adam Izdebski<sup>1,2,\*</sup>, Myriam Lizotte<sup>1,3</sup>, Kevin R. Moon<sup>4</sup>,  
 Jake S. Rhodes<sup>5</sup>, Guy Wolf<sup>1,3</sup>, and Ewa Szczerba<sup>1,6</sup>

<sup>1</sup>*Institute of AI for Health, Helmholtz Munich*

<sup>2</sup>*School of Computation, Information and Technology, Technical University of Munich*

<sup>3</sup>*Mila – Quebec AI Institute; Université de Montréal*

<sup>4</sup>*Dept. of Mathematics & Statistics, Utah State University*

<sup>5</sup>*Department of Statistics, Brigham Young University*

<sup>6</sup>*Faculty of Mathematics, Informatics and Mechanics, University of Warsaw*

## A Additional Methods

### A.1 Supervised Diffusion Geometry with RF-GAP Proximities

To construct a task-aware diffusion geometry aligned with the FDD framework, we use a supervised similarity kernel  $K(\mathbf{x}_i, \mathbf{x}_j)$  that defines pairwise affinities between samples  $\mathbf{x}_i, \mathbf{x}_j \in X$ . This kernel induces a local geometry on the input space  $X$  that is biased toward task-relevant structure.

In particular, we adopt random forest geometry- and accuracy-preserving (RF-GAP) proximities [27], which are derived from a random forest trained on the downstream task. RF-GAP proximities measure similarity between samples proportionally to the size of the terminal nodes they share across trees. These proximities can be used to construct a proximity-weighted nearest-neighbor classifier or regressor that exactly matches the performance of the random forest; hence, they capture the supervised geometry learned by the forest.

Formally, let  $B(t)$  be the multiset of in-bag sample indices in tree  $t$ ,  $J_i(t)$  the in-bag samples that share a terminal node with observation  $i$ ,  $c_j(t)$  the multiplicity of index  $j$  in  $B(t)$ ,  $M(t)$  the multiset of all in-bag observations in tree  $t$ , and  $S_i$  the set of trees for which observation  $i$  is out-of-bag. The RF-GAP proximity between observations  $i$  and  $j$  is defined as

$$K(\mathbf{x}_i, \mathbf{x}_j) = \frac{1}{|S_i|} \sum_{t \in S_i} \frac{c_j(t) \mathbf{1}(j \in J_i(t))}{|M(t)|}, \quad (\text{S1})$$

where  $\mathbf{1}(\cdot)$  denotes the indicator function. Collecting all pairwise proximities yields an affinity matrix  $\mathbf{K} \in \mathbb{R}^{N \times N}$  with entries  $K_{ij} = K(\mathbf{x}_i, \mathbf{x}_j)$ .

From  $\mathbf{K}$ , we define a diffusion operator  $\mathbf{P}$  via row normalization,

$$P_{ij} = \frac{K_{ij}}{\sum_l K_{il}}, \quad (\text{S2})$$

so that  $P_{ij}$  denotes the probability of a single-step transition from  $\mathbf{x}_i$  to  $\mathbf{x}_j$ . The matrix  $\mathbf{P}$  thus defines a Markov chain over the dataset, and repeated application of  $\mathbf{P}$  reveals geometry at multiple scales. The  $t$ -step transition matrix  $\mathbf{P}^t$  is used to define the discrete diffusion distance

$$D_t(\mathbf{x}_i, \mathbf{x}_j) = \sqrt{\sum_k \frac{(P_{ik}^t - P_{jk}^t)^2}{\phi(P_{kk})}}, \quad (\text{S3})$$

where  $\phi(P_{kk})$  denotes the stationary distribution of the Markov chain  $\mathbf{P}$ . Intuitively,  $D_t(\mathbf{x}_i, \mathbf{x}_j)$  is small when many short diffusion paths connect  $\mathbf{x}_i$  and  $\mathbf{x}_j$ ; the scale parameter  $t$  controls how local interactions are integrated into a multiscale geometric representation of the data manifold.

## A.2 Random Forest Autoencoder (RFAE)

The Random Forest Autoencoder (RFAE) provides a mechanism to embed new samples into this supervised diffusion geometry. During training, RFAE takes the RF-GAP proximity vector  $\mathbf{p}_n \in \mathbb{R}^N$  for each sample  $\mathbf{x}_n$  and learns a latent representation  $\mathbf{z}_n \in \mathbb{R}^d$  that preserves the manifold structure captured by RF-PHATE.

Let  $\mathbf{z}_n^G$  denote the RF-PHATE coordinates of sample  $\mathbf{x}_n$ , obtained by applying PHATE to the RF-GAP diffusion operator. RFAE uses an encoder  $f$  that maps proximities  $\mathbf{p}_n$  to latent codes  $\mathbf{z}_n = f(\mathbf{p}_n)$ , and a decoder  $g$  that reconstructs proximities  $\hat{\mathbf{p}}_n = g(\mathbf{z}_n)$ . By aligning  $\mathbf{z}_n$  with  $\mathbf{z}_n^G$ , RFAE learns an embedding that preserves diffusion distances while enabling parametric out-of-sample extension.

The training objective combines a reconstruction loss  $L_{\text{recon}}$  and a geometric alignment loss  $L_{\text{geo}}$  into a single composite loss:

$$L(f, g) = \frac{1}{N} \sum_{n=1}^N \left[ \lambda L_{\text{recon}}(\mathbf{p}_n, \hat{\mathbf{p}}_n) + (1 - \lambda) L_{\text{geo}}(\mathbf{z}_n, \mathbf{z}_n^G) \right]. \quad (\text{S4})$$

Here,  $L_{\text{recon}}$  is defined as the Kullback–Leibler divergence  $D_{\text{KL}}(\mathbf{p}_n \parallel \hat{\mathbf{p}}_n)$ , ensuring that reconstructed proximity distributions remain consistent with the RF-GAP similarities, and  $L_{\text{geo}}$  enforces correspondence between  $\mathbf{z}_n$  and the RF-PHATE embedding  $\mathbf{z}_n^G$ .

Through this joint reconstruction–alignment process, RFAE produces geometry-aware latent representations  $\mathbf{z}_n$  that generalize beyond the training set while retaining the discriminative and geometric properties of the supervised diffusion space. These diffusion-based embeddings serve as geometry-aware coordinates that can be further used within the FDD framework for prediction, retrieval, and decoding.

## B Diffusion for Visualization

### B.1 PHATE Kernel and Diffusion Operator

Following the idea of PHATE [23], we construct an affinity kernel that encodes local geometry in the pretrained embedding space. To mitigate issues faced by Gaussian kernels on sparsely sampled data, PHATE uses an adaptive bandwidth equal to the  $k$ -nearest-neighbor distance of each point, combined with an  $\alpha$ -decay that controls the rate of decay:

$$K_{k,\alpha}(\mathbf{x}_i, \mathbf{x}_j) = \frac{1}{2} \exp\left(-\left(\frac{\|\mathbf{x}_i - \mathbf{x}_j\|_2^2}{\varepsilon_k(\mathbf{x}_i)}\right)^\alpha\right) + \frac{1}{2} \exp\left(-\left(\frac{\|\mathbf{x}_i - \mathbf{x}_j\|_2^2}{\varepsilon_k(\mathbf{x}_j)}\right)^\alpha\right), \quad (\text{S5})$$

where  $\varepsilon_k(\mathbf{x}_i)$  is the distance from  $\mathbf{x}_i$  to its  $k$ -th nearest neighbor under the Euclidean norm.

Row-normalization of  $K_{k,\alpha}$  yields a diffusion operator  $\mathbf{P} \in \mathbb{R}^{N \times N}$  with entries

$$P_{ij} = \frac{K_{k,\alpha}(\mathbf{x}_i, \mathbf{x}_j)}{\sum_l K_{k,\alpha}(\mathbf{x}_i, \mathbf{x}_l)}, \quad (\text{S6})$$

so that  $P_{ij}$  defines a Markov diffusion process capturing single-step transitions within local data neighborhoods. Multi-step transitions are given by  $\mathbf{P}^t$ , which integrates local structure into multi-scale connectivity.

### B.2 RF-PHATE and RFAE for Supervised Visualization

RF-PHATE is a supervised extension of PHATE that uses a random forest trained on labels or task values to define the similarity kernel [26]. Instead of distances in the original feature space, RF-PHATE uses RF-GAP proximities as affinities, combining them with the PHATE machinery to obtain low-dimensional embeddings that emphasize task-relevant structure while suppressing irrelevant variation. Although RF-PHATE provides high-quality supervised visualizations, it does not directly support out-of-sample extension. RFAE [2] addresses this by training an autoencoder to reconstruct RF-GAP proximity vectors, as described above, while aligning its latent space with RF-PHATE coordinates. The resulting encoder  $f$  serves as a parametric mapping from new samples to supervised diffusion coordinates  $\mathbf{z}_n$ , which we leverage in the Diffuse step of FDD.

## C Hyperparameters for FDD

Component	Hyperparameter	Value	Description
RFAE	$n_{\text{components}}$	2	Dimensionality of the latent space.
	<code>pct_landmark</code>	None	Fraction of landmarks for Nyström approximation.
ODE integration	$t_{\text{start}}$	0.0	Initial time point.
	$t_{\text{end}}$	4.0	Final time point.
	$n_{\text{timepoints}}$	200	Number of discretization points.
	<code>solver</code>	<code>rk4</code>	ODE solver method.
OT Loss	<code>loss</code>	<code>sinkhorn</code>	Type of OT loss.
	$p$	2	Cost exponent.
	<code>blur</code>	0.002	Entropic regularization.
	<code>scaling</code>	0.9	Sinkhorn scaling.
NeuralODE	<code>num_epochs</code>	500	Maximum training epochs.
	<code>batch_size</code>	64	Mini-batch size.
	<code>lr</code>	$1 \times 10^{-4}$	Learning rate.
ManifoldMLP	<code>prox_dim</code>	1572	Input dimension (RFAE proximities).
	<code>emb_dim</code>	12800	Output dimension (Hyformer embeddings).
	<code>hidden_dims</code>	[8192, 12288]	Sizes of intermediate layers.
	<code>residual_scale</code>	0.3	Scaling in residual manifold projection.
MLP Training	<code>epochs</code>	300	Maximum training epochs.
	<code>patience</code>	20	Early-stopping patience.
	<code>optimizer</code>	<code>AdamW</code>	Optimizer type.
	<code>lr_start</code>	$3 \times 10^{-5}$	Base learning rate.
	<code>lr_max</code>	$5 \times 10^{-4}$	Peak learning rate.
	<code>weight_decay</code>	$1 \times 10^{-5}$	L2 regularization.
	<code>batch_size</code>	32	Mini-batch size.

Table S1: Hyperparameters for the FDD pipeline.